Tacrolimus Decreases Cognitive Function by Impairing Hippocampal Synaptic Balance: A Possible Role of Klotho

Yoo Jin Shin
Catholic University of Korea College of Medicine: Catholic University of Korea School of Medicine
Sun Woo Lim
Catholic University of Korea College of Medicine: Catholic University of Korea School of Medicine
Sheng Cui
Catholic University of Korea College of Medicine: Catholic University of Korea School of Medicine
Eun Jeong Ko
Catholic University of Korea College of Medicine: Catholic University of Korea School of Medicine
Byung Ha Chung
Catholic University of Korea College of Medicine: Catholic University of Korea School of Medicine
Hong Lim Kim
Catholic University of Korea College of Medicine: Catholic University of Korea School of Medicine
Tae Ryong Riew
Catholic University of Korea College of Medicine: Catholic University of Korea School of Medicine
Mun Yong Lee
Catholic University of Korea College of Medicine: Catholic University of Korea School of Medicine
CHUL WOO YANG (yangch@catholic.ac.kr)
Catholic University of Korea College of Medicine: Catholic University of Korea School of Medicine
https://orcid.org/0000-0001-9796-636X

Research Article

Keywords: Klotho, Cognitive dysfunction, Tacrolimus, Synaptic imbalance, Oxidative stress, Hippocampus

Posted Date: March 11th, 2021

DOI: https://doi.org/10.21203/rs.3.rs-280191/v1

Version of Record: A version of this preprint was published at Molecular Neurobiology on August 25th, 2021. See the published version at https://doi.org/10.1007/s12035-021-02499-3.

Abstract

The influence of long-term tacrolimus treatment on cognitive function remains to be elucidated. Using chronic tacrolimus neurotoxicity in mice, we evaluated the influence of tacrolimus on cognitive function, synaptic balance, its regulating protein (Klotho), and oxidative stress in the hippocampus. Compared to vehicle-treated mice, tacrolimus-treated mice showed significantly decreased hippocampal-dependent spatial learning and memory function. Furthermore, tacrolimus caused synaptic imbalance as demonstrated by decreased excitatory synapses and increased inhibitory synapses, and downregulated Klotho in a dose-dependent manner; its downregulation was localized to excitatory hippocampal synapses. Moreover, tacrolimus increased oxidative stress and was associated with the activation of the PI3K/AKT pathway in the hippocampus. The present results indicate that tacrolimus impairs cognitive function via synaptic imbalance, and that these processes are associated with Klotho downregulation at synapses through tacrolimus-induced oxidative stress in the hippocampus.

Introduction

Neurological alteration is a complication in one-third of organ transplant recipients after transplantation [1, 2]. Neurological complications such as cognitive, emotional, and behavioral changes in kidney transplant patients are associated with calcineurin inhibitors (CNIs), particularly chronic tacrolimus (TAC) treatment [3]; however, the causal relationship between TAC and impaired cognitive function remains unclear.

The hippocampus plays a pivotal role in cognitive functions including learning, memory, and spatial orientation [4, 5]. Learning and memory require interaction between new neurons and the hippocampal neural network. This process is based on synaptic plasticity, which is altered in response to synaptic neuronal activity [6].

Klotho, expressed in the brain and kidney, plays roles in anti-aging and cognitive function in the hippocampus and the brain [7, 8]. In animal studies, Klotho deficiency causes cognitive decline [9, 10], whereas Klotho overexpression leads to increased cognitive function [11]. In humans, Klotho levels in the cerebrospinal fluid decrease with aging in Alzheimer's disease [12], whereas Klotho upregulation enhances cognitive functions [11] in healthy individuals.

Moreover, Klotho possesses antioxidant functions and plays an important role in protecting against oxidative stress. Using Klotho$^{+/-}$ mice, we previously reported that Klotho deficiency renders the kidney more susceptible to TAC-induced oxidative stress [13] and that Klotho treatment inhibits the PI3K/AKT pathway, suggesting its essential role in protecting against CNI-induced oxidative stress. Thus, oxidative stress caused by long-term CNI exposure may affect cognitive function via Klotho in the hippocampus.

Here, to investigate the influence of TAC on cognitive function in the hippocampus, we evaluated hippocampal-dependent spatial memory function and the expression of related synapse markers and

neurotransmitter receptors in TAC-treated mice. Furthermore, we examined the spatiotemporal expression of Klotho in the hippocampus of TAC-treated mice.

Materials And Methods

Animal care and preparation

All animal procedures and experiments were approved by the Institutional Animal Care and Use Committee (IACUC) at the School of Medicine, Catholic University of Korea (CUMC-2020-0110-02) and conducted in accordance with the Laboratory Animals Welfare Act, the Guide for the Care and Use of Laboratory Animals, and the Guidelines and Policies for Rodent Experiments.
Eight-week-old male BALB/c mice (Orient Bio, Seongnam, South Korea), initially weighing 25–30 g, were housed with five animals/cage (Nalge, Rochester, NY, USA) under controlled conditions of temperature (20–26°C), humidity (50 ± 10%), and light (12-h light-dark cycle) at the animal care facility of the Catholic University of Korea.

To examine the effective dose of TAC-induced neurotoxicity, three different doses of TAC (Prograft, Astellas Pharma Inc., Ibaraki, Japan) diluted in olive oil (MilliporeSigma, Billerica, MA, USA) were subcutaneously injected into mice for 4 weeks. After 1-week acclimation, weight-matched mice were randomized into the following four groups (n = 10 per group): (1) vehicle (VH) receiving only olive oil at the same volume as the TAC groups, (2) TAC 1.5 receiving 1.5 mg/kg body weight of TAC in olive oil; (3) TAC 3, 3 mg/kg; (4) TAC 12, 12 mg/kg. The doses and duration of TAC administration were in accordance with our previous studies reporting that TAC causes organ damage including nephrotoxicity and neurotoxicity [14–16]. Further, the TAC concentration used in all experiments compared with the VH group was 3 mg/kg, the effective concentration for TAC-induced neurotoxicity.

Behavior tests

Open-field test

The open-field test (OFT) was performed to evaluate general locomotor activity in mice, as described previously with slight modification [17, 18]. Each mouse (n = 7) was placed in the center area of the OFT apparatus (50 × 50 × 38 cm^3), and its motility was observed during a 5-min period. Locomotor activity was measured from the total distance moved (cm), movement time (s), and velocity (cm/s), and was analyzed using a computerized video-tracking system with the SMART program (PanLab Co., Barcelona, Spain). After behavioral monitoring, the apparatus surface was cleaned with 70% ethanol solution and dried before testing the next animal.

Barnes maze test

The Barnes maze (BM) was used with slight modification [19] to evaluate spatial learning and memory functions in mice. To evaluate spatial learning and memory, mice were habituated to the BM through a training session (i.e., learning) for four consecutive days; the probe trial was then performed on day five.

Mice were placed in a light-blocked starting box at the center of the platform, which comprised four quadrants (the target quadrant including the escape hole, and the opposite quadrant, representatively) in the apparatus (diameter, 92 cm; height, 100 cm) with 20 holes located at the border. Only one escape hole was opened with a target box that was located under the escape hole, and the other 19 holes were closed. The starting box was removed after 10 s, and the mice were allowed to explore the platform. During 4 d, the mice were trained in spatial acquisition with four trials of 3 min at 20-min intervals. In the acquisition trials, mice that found the escape hole were placed in the target box for 60 s; those that did not find the escape hole for 3 min were gently guided to the target box. The escape latency of these mice was recorded as 180 s. On day 5, a probe trial was conducted for 90 s to evaluate the short-term memory of mice. The memory functions were indicated by the latency time (s) required to reach the escape hole, retention time at each quadrant of the platform, and the number of visits to the target hole. The BM test was performed using a computerized video-tracking system with the SMART program (PanLab Co.).

Tissue preparation

The experimental animals were anesthetized with tiletamine-zolazepam (10 mg/kg, intraperitoneal injection; Zoletil 50, Virbac Laboratories, Carros, France) and xylazine (15 mg/kg, intraperitoneal; Rompun®, Bayer, Leverkusen, Germany), and were then euthanized through transcardial perfusion with a fixative containing 4% paraformaldehyde in 0.1 M phosphate buffer (pH = 7.4) for 30 min or through decapitation. For histological evaluation, the brain was post-fixed in 4% paraformaldehyde for 4 h and then embedded in wax. For immunoblotting and reverse transcription-quantitative PCR (RT-qPCR) analyses, the hippocampus was separated and immediately frozen in liquid nitrogen. The samples were stored at -70°C until further use.

Immunofluorescence

Dewaxed 3-μm brain sections were incubated in retrieval solution (pH 6.0) and then washed in phosphate-buffered saline. After blocking with 10% normal donkey serum (Jackson ImmunoResearch, West Grove, PA, USA) for 1 h, the sections were incubated overnight at 4°C with a rabbit polyclonal antibody against Klotho (1:200; ab203576; Abcam, Cambridge, UK). Primary antibody binding was visualized using peroxidase-labeled donkey anti-rabbit IgG (1:100; Jackson ImmunoResearch) and 0.05% 3,3-diaminobenzidine tetrahydrochloride (DAB; Vector Laboratories, Burlingame, CA, USA) with 0.01% H_2O_2 as the substrate. For double or triple immunohistochemistry, the brain sections were incubated at 4°C overnight with the following antibodies: polyclonal guinea pig anti-vGlut1 (1:1000; #AB5905; Millipore Corp., Billerica, Mass., USA), monoclonal mouse antibody anti- PSD95 (1:200; MABN68; Millipore), MAP2 (1:400; M4403; MilliporeSigma), monoclonal rabbit antibody against gephyrin (1:200; AIP-005; Almone Labs, Jerusalem, Israel), β-3 tubulin (1:600; #5568; Cell Signaling Technology Inc., Danvers, MA, USA), polyclonal rabbit anti-Klotho antibody (Abcam) conjugated with biotinylated goat anti-rabbit IgG (BA-1000; Vector Laboratories Inc.), and 8-Hydroxy-2'-deoxyguanosine (1:200; 8-OHdG; MOG-100P; Japan Institute for the Control of Aging, Shizuoka, Japan). Antibody staining was visualized using the following secondary antibodies: Dichlorotriazinylamino fluorescein (DTAF)-conjugated streptavidin (1:100; Jackson ImmunoResearch), Cy3-conjugated goat anti-rabbit antibody (1:1000; Jackson ImmunoResearch), Cy3-

conjugated goat anti-mouse antibody (1:1000; Jackson ImmunoResearch), Alexa Fluor 488-conjugated goat anti-guinea pig antibody (1:200; Thermo Fisher, Waltham, MA, USA), Alexa Fluor 488-conjugated goat anti-mouse antibody (1:200; Thermo Fisher), or Alexa Fluor 647-conjugated goat anti-mouse antibody (1:200; Thermo Fisher). Cell nuclei were then counterstained with 4,6-diamidino-2-phenylindole (DAPI; Roche, Mannheim, Germany) for 10 min.

Slides were observed using a confocal microscope (LSM700; Carl Zeiss Co. Ltd., Oberkochen, Germany). Images were converted to the TIFF format, and contrast levels were adjusted using Adobe Photoshop v. 13 (Adobe System, San Jose, CA, USA). The IMARIS program (Bitplane, Zurich, Switzerland) was used for three-dimensional (3D) rendered Z-stacked confocal images.

Immunoelectron microscopic analysis

Small blocks (1–2 mm^2) of mouse hippocampal CA1 regions were cryopreserved by immersing in 2.3 M sucrose and were frozen in liquid nitrogen. Frozen tissues were cut with 2-μm-thick semithin cryosections using a glass knife in a Leica EM UC7 ultramicrotome equipped with an FC7 cryochamber (Leica, Wetzlar, Germany).

For pre-embedding immuno-EM, the sections were incubated at 4°C overnight with polyclonal rabbit anti-Klotho antibody (1:200; Abcam). The sections were then labeled with peroxidase-conjugated goat anti-rabbit IgG (1:100; Jackson ImmunoResearch) for immunoperoxidase staining, or with nanogold particle (1 nm)-conjugated anti-rabbit secondary antibody (1:100; Nanoprobes, Stony Brook, NY, USA) for immunogold/silver staining. Each Klotho-labeled tissue was visualized using 0.05% DAB as a chromogen for peroxidase, or a silver enhancement kit (Nanoprobes) for nanogold-conjugated antibodies. After postfixation, dehydration, and embedding in Epon 812 (Polysciences, Warrington, PA, USA), the areas of interest were excised and glued onto resin blocks. Ultra-thin sections (70 nm thick) were cut and observed under an electron microscope (JEM 1010, JEOL, Tokyo, Japan) after uranyl acetate staining.

Correlative EM was performed as previously described [20].

Semithin cryosections were incubated with a mixture of polyclonal rabbit anti-Klotho antibody (1:200; Abcam) and monoclonal mouse antibody anti-MAP2 (1:400; MilliporeSigma), followed by Alexa Fluor 488-conjugated goat anti-rabbit antibody (1:200; Thermo Fisher) and Cy3-conjugated goat anti-mouse (1:1000; Jackson ImmunoResearch).
The sections were then labeled with DAPI to counterstain the cell nuclei. The stained sections were covered with coverslips and examined using a confocal microscope for fluorescence. Differential interference contrast settings were used to identify the region of interest in the sections through EM. The coverslips were then removed, and the sections were processed for EM as described above.

Immunoblotting

Frozen hippocampal tissues were homogenized in Pro-Prep Protein Extraction Solution (Intron Biotechnology, Seongnam, South Korea) per the manufacturer's protocol. Equimolar amounts (20 μg) of

protein were separated through SDS-PAGE and electroblotted onto a polyvinylidene fluoride membranes (Millipore). The membranes were incubated overnight at 4°C with the following antibodies: polyclonal rabbit anti-Klotho antibody (1:1000; Abcam), p-AKT (Ser473) (1:1000; #9271S; Cell Signaling Technology Inc.), t-AKT (1:1000; #9272 S; Cell Signaling Technology Inc.), p-FoxO3a (Ser253) (1:1000; #9466 S; Cell Signaling Technology Inc.), t-FoxO3a (1:1000; #2497S; Cell Signaling Technology Inc.), SOD/MnSOD (1:1000; ab13533; Abcam), monoclonal rabbit anti-gephyrin (1:1000; Almone Labs), polyclonal guinea pig anti-vGlut1 (1:1000; #AB5905; Millipore), monoclonal mouse anti-VGAT (1:1000; 131 011; Synaptic System), PSD95 (Millipore), and monoclonal mouse anti-β-actin (1:10000; A5441; Sigma-Aldrich). The immunoreactive bands were detected using a chemiluminescence kit (ATTO Corporation, Tokyo, Japan). Each band was quantified by relative density as a percentage of the ratio of the TAC group to that of the VH group, and each density was normalized to that of β-actin (Quantity One version 4.4.0; Bio-Rad, Hercules, CA, USA).

RT-qPCR

Total RNA from the mouse hippocampus samples was extracted using RNA isolation reagent (RNA-Bee; Tel Test, Inc., TX, USA). The purified RNA (5 μg) was reverse transcribed into first-strand complementary DNA using a Dyne 1st -Strand cDNA Synthesis Kit (DyneBio Inc., Seongnam, Korea). RT-qPCR amplification was conducted using SYBR Green PreMix in a LightCycler 480 system (Roche, Rotkreuz, Switzerland). The mRNA expression level was normalized to that of GAPDH using the change in the cycle threshold method. The following primers were used for qPCR: 5'-AAAAGTCGGGGTCTCTCTGAC-3' and 5'-CAGTCGGTCCAAAATTCTTGTGA-3' for mouse GABA A receptor subunit alpha 1 (GABARA1), 5'-TTACAGTCCAAGCCGAATGTCCC-3' and 5'-ACTTCTGAGGTTGTGTAAGCGTAGC-3' for mouse GABA A receptor subunit alpha 2 (GABARA2), 5'-CAAGAACCTGGGGACTTTGTGAA-3' and 5'-AGCCGATCCAAGATTCTAGTGAA-3' for mouse GABA A receptor subunit alpha 3 (GABARA3), 5'-GAGACTGGTGGATTTTCCTATGG-3' and 5'-GGTCCAGGTGTAGATCATCTCACT-3' for mouse GABA A receptor subunit alpha 4 (GABARA4), 5'-CCCTCCTTGTCTTCTGTATTTCC-3' and 5'-TGATGTTGTCATTGGTCTCGTCT-3' for mouse GABA A receptor subunit alpha 5 (GABARA5), 5'-ATCTGCCTGGTTCCATGATGT-3' and 5'-AGCCATAGCTCTCTAGGTCCA-3' for mouse GABA A receptor subunit delta (GABARD), 5'-AGAAAAACCCTCTTCTTCGGATG-3' and 5'-GTGGCATTGTTCATTTGAATGGT-3' for mouse GABA A receptor subunit gamma 2 (GABARG2), 5'-CTCGCCCTTGTCGTACCAC-3' and 5'-GTCCGCCCTGAGAAATCCAG-3' for mouse AMPA receptor subunit 1 (GluR1), 5'-GTGTCGCCCATCGAAAGTG-3' and 5'-AGTAGGCATACTTCCCTTTGGAT-3' for mouse AMPA receptor subunit 2 (GluR2), 5'-ATCGGATATTCGCAAGGAACC-3' and 5'-CCATAGGGCCAGATTCCACA-3' for mouse kainate receptor subunit 1 (GluR6), 5'-AAAGGCCAGAGGTCCAACTAT-3' and 5'-CCCCTTCAGCATTAAGTATGGGT-3' for mouse kainate receptor subunit 4 (KAR1), 5'-ATAGTCGCCTTCGCCAATCC-3' and 5'-GTGTCCGTGGTCTCGTACTG-3' for mouse kainate receptor subunit 5 (KAR2), 5'-AGAGCCCGACCCTAAAAAGAA-3' and 5'-CCCTCCTCCCTCTCAATAGC-3' for mouse NMDA receptor subunit 1 (NR1), 5'-TGATGAACCGCACTGACCCTA-3' and 5'-TGGGGATGAAAGTCTGTGAGG-3' for mouse NMDA receptor subunit alpha 2 (NR2A), 5'-GCCATGAACGAGACTGACCC-3' and 5'-GCTTCCTGGTCCGTGTCATC-3' for mouse NMDA receptor subunit beta 2 (NR2B), 5'-

AGGTCCTAATGTCACTGACTCTC-3' and 5'-GCCATAAAGGGTCCTATCAGAC-3' for mouse metabolic glutamate receptor subunit 7 (mGluR7), and 5'-AGGTCGGTGTGAACGGATTTG-3' and 5'-TGTAGACCATGTAGTTGAGGTCA-3' for mouse Gapdh. All experiments were performed in triplicate on samples from individual mice (n = 4).

Quantitative and statistical analysis

Klotho-labeling profiles and other synapse markers were evaluated by counting approximately 20 randomly selected areas (50 × 50 μm^2 per field) in each stained tissue section at ×400 magnification using a color image analyzer (TDI Scope Eye, version 3.0, for Windows).

All data are presented as the mean ± standard error; unpaired t-tests or one-way ANOVA followed by the Bonferroni post hoc test were used for comparing among groups.
Differences with P-values less than 0.05 were considered significant. All statistical analyses were conducted using GraphPad Prism version 5 (GraphPad Software Inc., San Diego, CA, USA).

Results

Effects of TAC treatment on cognitive function in mice

We performed behavioral analysis to evaluate whether TAC impairs cognitive function in mice. We used TAC at 3 mg/kg body weight as previously reported [14–16]. First, locomotor activity in VH and TAC groups was examined using the OFT. There was no significant difference in the total distance moved, movement time, and velocity, indicating similar locomotion between the two groups (Fig. 1A).

Spatial learning performance and memory were then examined using the BM. During the four acquisition trial days, the latency time to the escape hole was gradually decreased in both groups; however, the TAC group showed longer latency time than that of the VH group (Fig. 1B) (day 1, 81.1 ± 4 s for VH, 86.7 ± 1.4 s for TAC; day 2, 42.9 ± 3.9 s for VH, 60.3 ± 6.7 s for TAC; day 3, 31.2 ± 2.4 s for VH, 57.6 ± 6.7 s for TAC; day 4, 23.1 ± 0.8 s for VH, 46.9 ± 3.2 s for TAC). On day 5, the probe trial day, TAC-treated mice spent less time in the target quadrant (56.9 ± 2.8 % for VH; 21.4 ± 3.4 % for TAC) and more time in the opposite quadrant compared (14.7 ± 3.2 % for VH; 36.2 ± 6.6 % for TAC) to VH mice (Fig. 1C); further, the TAC group showed increased primary latency time (22.7 ± 1.5 s for VH; 45.9 ± 3.5 s for TAC) and distance of movement, and a decreased number of visits to the escape hole (10.3 ± 2.2 for VH; 5.7 ± 0.7 for TAC) compared with the VH group (Fig. 1D–F). These findings suggest that TAC treatment significantly influenced cognitive function in mice, resulting in impaired spatial learning and memory.

Effects of TAC treatment on synapses

First, we investigated the effects of TAC treatment on synaptic changes in the mouse hippocampus, using excitatory- (vGlut1 and PSD95; Fig. 2A, C, E) and inhibitory synaptic markers (VGAT and gephyrin; Fig. 2B, D, F), respectively. TAC-treated mice showed decreased immunoreactive puncta for excitatory synapse markers vGlut1 and PSD95 (Fig. 2A) (vGlut1, 160 ± 5.5 for VH, 91.3 ± 4.4 for TAC; PSD95, 758.2

± 17.7 for VH, 371.8 ± 14.9 for TAC); vGlut1/PSD95 co-labeled puncta were also decreased by TAC treatment (Fig. 2C) (307.8 ± 19.6 for VH, 125.4 ± 12.1 for TAC). In contrast, immunoreactive puncta for inhibitory synapse markers VGAT and gephyrin were increased upon TAC treatment (Fig. 2B) (VGAT, 31.3 ± 2.1 for VH, 63.8 ± 2.9 for TAC; gephyrin, 85.4 ± 6.9 for VH, 148.6 ± 9.9 for TAC), and VGAT/gephyrin co-labeled puncta were decreased (Fig. 2D) (11.6 ± 1.3 for VH, 48 ± 3.9 for TAC).

On immunoblotting for excitatory synapse markers vGlut1 and PSD95 (Fig. 2E) and inhibitory synapse markers VGAT and gephyrin (Fig. 2F), the immunoreactive bands of each synapse marker were quantified and compared in both VH and TAC groups. The labeling intensity of excitatory synapses was remarkably decreased, whereas inhibitory synapses ere increased in the TAC group compared to the VH group. Furthermore, RT-qPCR analysis revealed that glutamate receptors were significantly downregulated, whereas GABAergic receptors were upregulated in the TAC group compared to the VH group (Fig. 3).

Influence of TAC treatment on Klotho expression in hippocampus

As TAC treatment impaired cognitive function in mice, we examined the changes in Klotho. First, we evaluated the distribution of Klotho expression and the influence of TAC on hippocampal Klotho expression. Klotho was expressed in the pyramidal neurons in the hippocampal CA1 region on immunohistochemistry (Fig. 4A), consistent with a previous report [21]. Immunoblotting for hippocampal proteins revealed that the Klotho antibody was detected as a single band at ~ 130 kDa in both VH and TAC groups (Fig. 4B). The labeling intensity of Klotho in the hippocampus was remarkably decreased in a dose-dependent manner (61.1 ± 4.6 % for TAC 1.5; 52.2 ± 8.6 % for TAC 3; 43.7 ± 4.8 % for TAC 12) in the TAC-treated groups compared with that of the VH group (100 ± 4.3 %).

Second, we identified the phenotype of Klotho expression in the CA1 region, a particularly vulnerable area in the hippocampus (boxed area in Fig. 1A), and evaluated the influence of TAC on Klotho expression in neuronal cells. Triple labeling was performed using Klotho and the neuronal markers, β-III tubulin and microtubule-associated protein 2 (MAP2). Most Klotho expression in the pyramidal cell layer (pcl) was detected in preserved neurons showing β-III tubulin and MAP2 immunoreactivity with neuronal processes elongated to the stratum radiatum (sr) (Fig. 4C – D). Prominent neuronal Klotho expression, including the soma and neurites, was observed in the VH group (Fig. 4C and E – H), whereas the TAC group showed weak Klotho immunoreactivity in the neurons (Fig. 4D, and I – L).

Influence of TAC treatment on Klotho expression in neuronal dendrites

As shown in Fig. 4E and I, Klotho immunoreactivity was observed in neuronal processes and neurites. We then performed double labeling for Klotho and MAP2, a marker specific for neuronal dendrites. MAP2-positive dendrites showed prominent Klotho expression with punctate structures along the dendritic processes (Fig. 5A, C). In particular, Klotho was localized along the outer part of the dendrite, indicating

presumptive synapse structures, identified through 3D reconstruction (Fig. 5B, D) of their morphology and topographical distribution. Quantitative analysis revealed significantly lesser Klotho-expressing puncta in the TAC group than in the VH group (Fig. 5E).

Localization of Klotho in neuronal dendrites

Klotho expression in MAP2-immunoreactive neuronal dendrites was first observed through confocal microscopy (Fig. 6A – C), and the same sections from these images were subjected to electron microscopy (Fig. 6D – E). Electron microscopy revealed presynaptic vesicles (white asterisks in Fig. 6F) and adjacent postsynaptic density (PSD) (arrowheads in Fig. 6F), an electron-dense structure at the postsynaptic membrane [22]. Klotho immunoreactivity indicated by electron-dense DAB grains (black asterisks in Fig. 6G) or silver-enhanced gold particles (arrows in Fig. 6H) was revealed in pre-embedding immunoelectron microscopic images. Reactive Klotho was detected in the postsynaptic profiles including the PSD (arrowheads in Fig. 6G – H), and composed the junction along with the vesicle-containing presynapses (white asterisks in Fig. 6G – H).

Effects of TAC treatment on synaptic Klotho expression

Furthermore, we investigated the involvement of Klotho in inhibitory and excitatory synapses after TAC treatment. As Klotho is localized in postsynapses, we performed double labeling for Klotho and an excitatory postsynaptic marker (PSD95; Fig. 7A-F) or for Klotho and an inhibitory postsynaptic marker (gephyrin; Fig. 7H-M). Confocal microscopic images (Fig. 7A – B, D – E, H – I, K – L) of reactive Klotho-, PSD95-, and gephyrin-positive puncta were 3D reconstructed (Fig. 7C, F, J, M) using IMARIS and the number of Klotho-expressing synapses in total synapses was quantified. Klotho/PSD95 co-labeled puncta were lesser after TAC treatment (224.8 ± 5.4 for VH, 88 ± 2.2 for TAC); the rate of double-labeled expression in total PSD95-positive excitatory postsynapses was also decreased significantly (0.3 ± 0.005 for VH, 0.24 ± 0.006 for TAC) (Fig. 7G). In contrast, Klotho/gephyrin co-labeled puncta were increased (64.3 ± 5.6 for VH, 106.6 ± 3.5 for TAC) in TAC-treated mice; however, the proportion of double-labeled expression in total gephyrin-positive inhibitory postsynapses was retained in both groups (0.77 ± 0.05 for VH, 0.75 ± 0.02 for TAC) (Fig. 7M).

Effects of TAC treatment on oxidative stress in the hippocampus

To investigate whether Klotho downregulation is associated with oxidative stress regulation after TAC treatment, we double labeling for Klotho and 8-OHdG, a marker of cellular oxidative DNA damage, in the hippocampus. The nuclear immunoreactivity of 8-OHdG in weak Klotho-expressing neurons was remarkably greater in the TAC group than in the VH group (Fig. 8A – H). Further, since the antioxidant effects of Klotho are regulated by MnSOD signaling [23–25], we examined the increased oxidative stress in the hippocampus of TAC-treated mice through immunoblotting for AKT, FoxO3a, and MnSOD (Fig. 8I–

J). Consistent with Klotho downregulation in TAC-treated mice, p-AKT and p-FoxO3a were upregulated, whereas MnSOD, a FoxOs target gene, was downregulated.

Discussion

Our results clearly indicate that long-term TAC treatment impairs cognitive function. Using an experimental model of chronic TAC neurotoxicity, we confirmed that chronic TAC treatment in mice caused cognitive dysfunction and impaired spatial learning and memory function. TAC treatment caused synaptic imbalance and downregulated Klotho in the hippocampus. These findings indicate that TAC decreases cognitive function by impairing hippocampal synaptic plasticity and that Klotho is involved in this process.

Hippocampal function is based on synapses that regulate the excitation-inhibition balance; the excitatory-to-inhibitory input ratio remains constant and is conserved under normal conditions [26–31]. We examined synaptic changes in the mouse hippocampus using the excitatory and inhibitory synaptic markers. TAC treatment decreased the number of excitatory synapses and increased the number of inhibitory synapses. These changes were also observed at the protein and mRNA levels. These findings suggest that TAC causes synaptic imbalance in the hippocampus.

Klotho plays an important role in cognitive function in the hippocampus [8, 10, 11, 32, 33]. However, the localization of Klotho in the synapse remains unclear. Thus, we evaluated the distribution of Klotho expression in the hippocampus. On examining the hippocampal CA1 region, identifying the phenotype of Klotho-expressing cells, and examining the subcellular localization of Klotho, we found that Klotho was expressed in neuronal processes and was localized to the postsynaptic neurites at the subcellular level.

To our knowledge, this is the first report on the anatomical localization of Klotho expression in the synapse.

Next, the influence of TAC on the changes in Klotho were examined. TAC downregulated hippocampal Klotho in a dose-dependent manner. As previously reported [21], Klotho expression was localized in hippocampal neurons, and TAC treatment downregulated Klotho in neurons. Further, TAC treatment downregulated Klotho at excitatory but not inhibitory synapses. Thus, TAC downregulates Klotho at the synapses in hippocampal neurons.

Overall, these findings suggest that TAC causes synaptic imbalance in the hippocampus, and Klotho downregulation is potentially involved in this process. Thus far, the effect of Klotho on synaptic function remains unclear. We thus speculate that Klotho regulates the balance between input and output signals, and Klotho downregulation at excitatory synapses results in synaptic imbalance. Overall, we propose that TAC-induced impairment of cognitive function is associated with synaptic imbalance via Klotho downregulation at hippocampal excitatory synapses.

Using Klotho$^{+/-}$ mice, we previously reported that Klotho deficiency renders the kidney more susceptible to TAC-induced injury, which is closely associated with aggravated TAC-induced oxidative stress [13, 34]. This study investigated whether TAC-induced oxidative stress affects hippocampal Klotho expression. Klotho is an important regulator of oxidative stress, and its effect is associated with the PI3K-Akt-FoxOs signaling pathway [9, 13, 35–37]. Our results indicate that TAC increased 8-OHdG, an oxidative damage marker, activated PI3K/AKT-mediated phosphorylation of FoxO3a, and inhibited FoxO3a binding to the MnSOD promoter, leading to reduced MnSOD expression (Fig. 7I-J). Thus, TAC-induced oxidative stress downregulated Klotho via PI3K/AKT pathway activation in the hippocampus.

CNI treatment is associated with neurotoxicity [38]. However, the influence of CNIs on cognitive function remains controversial [39–43], possibly owing to the diverse etiology of cognitive impairment after organ transplantation, including age underlying disease. Our study clearly defines the association between CNI and cognitive function. Impaired cognitive function in organ transplant recipients results in hindrances in daily living (including medication adherence) and increased morbidity and mortality. However, the importance of cognitive function has been overlooked thus far. Our study indicates the importance of evaluating cognitive function in organ transplant recipients with long-term exposure to CNIs.

Our study defines the association between Klotho expression and TAC-induced cognitive dysfunction; however, it did not include a functional study. Nonetheless, it suggests that decreased cognitive function by TAC is causally associated with Klotho downregulation in the hippocampus. Thus, further studies using Klotho-deficient or -overexpressing mice are needed to determine the role of Klotho at the synaptic level.

In summary, our data indicate that TAC treatment impairs cognitive function via synaptic imbalance in the hippocampus, and that these processes may be associated with Klotho downregulation through TAC-induced oxidative stress (Fig. 9).

Declarations

Authors' Contributions

YJ Shin, SW Lim, and CW Yang; designed the research and wrote the report; YJ Shin, and C Sheng: conducted the animal experiments; EJ Ko, TR Riew, and HL Kim: performed the histological experiments; YJ Shin, BH Chung, MY Lee, and CW Yang; analyzed the data and edited the manuscript.

Funding

This work was supported by the Korean Health Technology R&D Project, Ministry for Health & Welfare, Republic of Korea (HI14C3417), and the Basic Science Research Program through a National Research Foundation of Korea (NRF) grant funded by the Ministry of Education (NRF-2018R1D1A1B07044219) and the Ministry of Science, ICT & Future Planning (NRF- 2020R1A2C2012711).

Data Availability

The data that support the findings of this study are available from the corresponding author upon reasonable request.

Declarations

Conflict of interest

The authors of this manuscript have no conflicts of interests.

Ethical Approval

This study was approved by the Institutional Animal Care and Use Committee (IACUC) at the School of Medicine, Catholic University of Korea (CUMC-2020-0110-02).

Consent to Participate

Not applicable

Consent for Publication

Not applicable

References

1. Zivkovic S (2007) Neuroimaging and neurologic complications after organ transplantation. J Neuroimaging 17:110–123
2. Zivkovic SA, Abdel-Hamid H (2010) Neurologic manifestations of transplant complications. Neurol Clin 28:235–251
3. Gijtenbeek JM, van den Bent MJ, Vecht CJ (1999) Cyclosporine neurotoxicity: a review. J Neurol 246:339–346
4. Eichenbaum H, Otto T, Cohen NJ (1992) The hippocampus–what does it do? Behav Neural Biol 57:2–36
5. Olton DS, Walker JA, Gage FH (1978) Hippocampal connections and spatial discrimination. Brain Res 139:295–308
6. Kennedy MB (2013) Synaptic Signaling in Learning and Memory. Cold Spring Harb Perspect Biol 8:a016824
7. Abraham CR, Mullen PC, Tucker-Zhou T, Chen CD, Zeldich E (2016) Klotho Is a Neuroprotective and Cognition-Enhancing Protein. Vitam Horm 101:215–238
8. Clinton SM, Glover ME, Maltare A, Laszczyk AM, Mehi SJ, Simmons RK, King GD (2013) Expression of klotho mRNA and protein in rat brain parenchyma from early postnatal development into

adulthood. Brain Res 1527:1–14

9. Kuro-o M, Matsumura Y, Aizawa H, Kawaguchi H, Suga T, Utsugi T, Ohyama Y, Kurabayashi M et al (1997) Mutation of the mouse klotho gene leads to a syndrome resembling ageing. Nature 390:45–51
10. Nagai T, Yamada K, Kim HC, Kim YS, Noda Y, Imura A, Nabeshima Y, Nabeshima T (2003) Cognition impairment in the genetic model of aging klotho gene mutant mice: a role of oxidative stress. FASEB J 17:50–52
11. Dubal DB, Yokoyama JS, Zhu L, Broestl L, Worden K, Wang D, Sturm VE, Kim D et al (2014) Life extension factor klotho enhances cognition. Cell Rep 7:1065–1076
12. Semba RD, Moghekar AR, Hu J, Sun K, Turner R, Ferrucci L, O'Brien R (2014) Klotho in the cerebrospinal fluid of adults with and without Alzheimer's disease. Neurosci Lett 558:37–40
13. Jin J, Jin L, Lim SW, Yang CW (2016) Klotho Deficiency Aggravates Tacrolimus-Induced Renal Injury via the Phosphatidylinositol 3-Kinase-Akt-Forkhead Box Protein O Pathway. Am J Nephrol 43:357–365
14. Hwang H, Ghee JY, Song JH, Piao S, Yang CW (2012) Comparison of adverse drug reaction profiles of two tacrolimus formulations in rats. Immunopharmacol Immunotoxicol 34:434–442
15. Lim SW, Jin L, Luo K, Jin J, Shin YJ, Hong SY, Yang CW (2017) Klotho enhances FoxO3-mediated manganese superoxide dismutase expression by negatively regulating PI3K/AKT pathway during tacrolimus-induced oxidative stress. Cell Death Dis 8:e2972
16. Shin YJ, Chun YT, Lim SW, Luo K, Quan Y, Cui S, Ko EJ, Chung BH et al (2019) Influence of Tacrolimus on Depressive-Like Behavior in Diabetic Rats Through Brain-Derived Neurotrophic Factor Regulation in the Hippocampus. Neurotox Res 36:396–410
17. Damian JP, Acosta V, Da Cuna M, Ramirez I, Oddone N, Zambrana A, Bervejillo V, Benech JC (2014) Effect of resveratrol on behavioral performance of streptozotocin-induced diabetic mice in anxiety tests. Exp Anim 63:277–287
18. Lee B, Sur B, Yeom M, Shim I, Lee H, Hahm DH (2014) L-tetrahydropalmatine ameliorates development of anxiety and depression-related symptoms induced by single prolonged stress in rats. Biomol Ther (Seoul) 22:213–222
19. Pompl PN, Mullan MJ, Bjugstad K, Arendash GW (1999) Adaptation of the circular platform spatial memory task for mice: use in detecting cognitive impairment in the APP(SW) transgenic mouse model for Alzheimer's disease. J Neurosci Methods 87:87–95
20. Riew TR, Kim HL, Choi JH, Jin X, Shin YJ, Lee MY (2017) Progressive accumulation of autofluorescent granules in macrophages in rat striatum after systemic 3-nitropropionic acid: a correlative light- and electron-microscopic study. Histochem Cell Biol 148:517–528
21. Li Q, Vo HT, Wang J, Fox-Quick S, Dobrunz LE, King GD (2017) Klotho regulates CA1 hippocampal synaptic plasticity. Neuroscience 347:123–133
22. Palay SL (1956) Synapses in the central nervous system. J Biophys Biochem Cytol 2:193–202

23. Brunet A, Bonni A, Zigmond MJ, Lin MZ, Juo P, Hu LS, Anderson MJ, Arden KC et al (1999) Akt promotes cell survival by phosphorylating and inhibiting a Forkhead transcription factor. Cell 96:857–868
24. Kops GJ, Dansen TB, Polderman PE, Saarloos I, Wirtz KW, Coffer PJ, Huang TT, Bos JL et al (2002) Forkhead transcription factor FOXO3a protects quiescent cells from oxidative stress. Nature 419:316–321
25. Zhang X, Tang N, Hadden TJ, Rishi AK (2011) Akt, FoxO and regulation of apoptosis. Biochim Biophys Acta 1813:1978–1986
26. Anderson JS, Carandini M, Ferster D (2000) Orientation tuning of input conductance, excitation, and inhibition in cat primary visual cortex. J Neurophysiol 84:909–926
27. Atallah BV, Scanziani M (2009) Instantaneous modulation of gamma oscillation frequency by balancing excitation with inhibition. Neuron 62:566–577
28. Cline H (2005) Synaptogenesis: a balancing act between excitation and inhibition. Curr Biol 15:R203–R205
29. Iascone DM, Li Y, Sumbul U, Doron M, Chen H, Andreu V, Goudy F, Blockus H et al (2020) Whole-Neuron Synaptic Mapping Reveals Spatially Precise Excitatory/Inhibitory Balance Limiting Dendritic and Somatic Spiking. Neuron 106:566–578 e568
30. Okun M, Lampl I (2008) Instantaneous correlation of excitation and inhibition during ongoing and sensory-evoked activities. Nat Neurosci 11:535–537
31. Wehr M, Zador AM (2003) Balanced inhibition underlies tuning and sharpens spike timing in auditory cortex. Nature 426:442–446
32. Degaspari S, Tzanno-Martins CB, Fujihara CK, Zatz R, Branco-Martins JP, Viel TA, Buck Hde S, Orellana AM et al (2015) Altered KLOTHO and NF-kappaB-TNF-alpha Signaling Are Correlated with Nephrectomy-Induced Cognitive Impairment in Rats. PLoS One 10:e0125271
33. Park SJ, Shin EJ, Min SS, An J, Li Z, Hee Chung Y, Hoon Jeong J, Bach JH et al (2013) Inactivation of JAK2/STAT3 signaling axis and downregulation of M1 mAChR cause cognitive impairment in klotho mutant mice, a genetic model of aging. Neuropsychopharmacology 38:1426–1437
34. Honda T, Hirakawa Y, Nangaku M (2019) The role of oxidative stress and hypoxia in renal disease. Kidney Res Clin Pract 38:414–426
35. Kokkinaki M, Abu-Asab M, Gunawardena N, Ahern G, Javidnia M, Young J, Golestaneh N (2013) Klotho regulates retinal pigment epithelial functions and protects against oxidative stress. J Neurosci 33:16346–16359
36. Kuro-o M (2011) Klotho and the aging process. Korean J Intern Med 26:113–122
37. Rakugi H, Matsukawa N, Ishikawa K, Yang J, Imai M, Ikushima M, Maekawa Y, Kida I et al (2007) Anti-oxidative effect of Klotho on endothelial cells through cAMP activation. Endocrine 31:82–87
38. DiMartini A, Crone C, Fireman M, Dew MA (2008) Psychiatric aspects of organ transplantation in critical care. Crit Care Clin 24:949–981

39. Grimm M, Yeganehfar W, Laufer G, Madl C, Kramer L, Eisenhuber E, Simon P, Kupilik N et al (1996) Cyclosporine may affect improvement of cognitive brain function after successful cardiac transplantation. Circulation 94:1339–1345
40. Griva K, Hansraj S, Thompson D, Jayasena D, Davenport A, Harrison M, Newman SP (2004) Neuropsychological performance after kidney transplantation: a comparison between transplant types and in relation to dialysis and normative data. Nephrol Dial Transplant 19:1866–1874
41. Martinez-Sanchis S, Bernal MC, Montagud JV, Candela G, Crespo J, Sancho A, Pallardo LM (2011) Effects of immunosuppressive drugs on the cognitive functioning of renal transplant recipients: a pilot study. J Clin Exp Neuropsychol 33:1016–1024
42. Padovan CS, Yousry TA, Schleuning M, Holler E, Kolb HJ, Straube A (1998) Neurological and neuroradiological findings in long-term survivors of allogeneic bone marrow transplantation. Ann Neurol 43:627–633
43. Scherwath A, Schirmer L, Kruse M, Ernst G, Eder M, Dinkel A, Kunze S, Balck F et al (2013) Cognitive functioning in allogeneic hematopoietic stem cell transplantation recipients and its medical correlates: a prospective multicenter study. Psychooncology 22:1509–1516

Figures

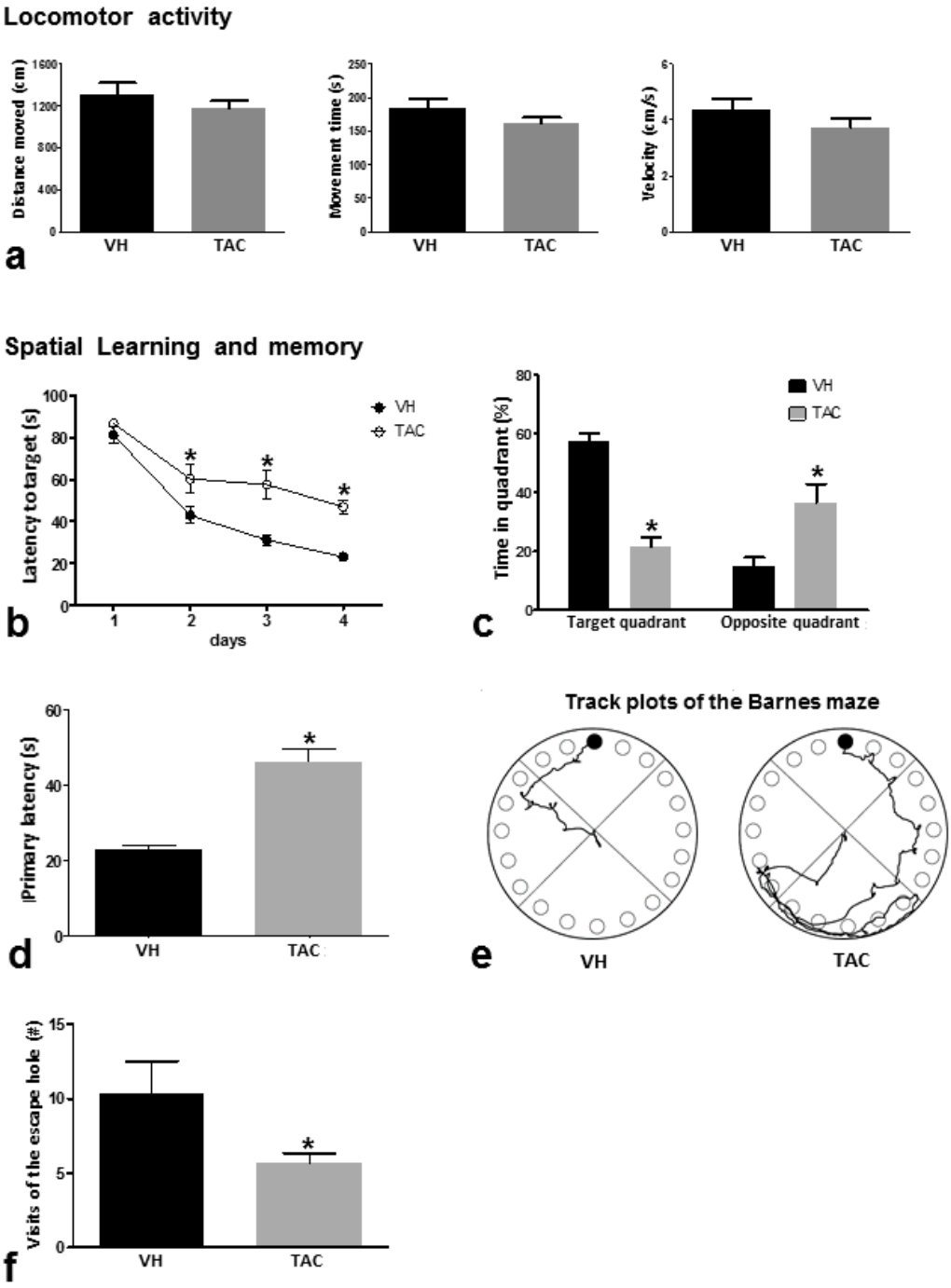

Figure 1

Chronic TAC treatment affects spatial learning performance and memory in mice. (A) Distance moved (cm), movement time (s), and velocity (cm/s) were examined in the open-field box for assessing locomotor activity. No difference in locomotion was observed between the VH and TAC-treated mice. (B) Total latency time required to find the target hole during the training sessions (Day 1-4). (C–F) During the probe trial (Day 5), spatial memory was evaluated by measuring the time spent in the target and opposite

quadrants (C), the primary latency (D), the distance moved (E), and the number of visits to the target hole (F). (E) Representative images showing the tracing path of VH- and TAC-treated mice in the Barnes maze. The TAC group showed significant impairment of spatial learning and memory compared with the VH group. The values shown are the mean ± SE (n = 7). *P < 0.05 vs. VH.

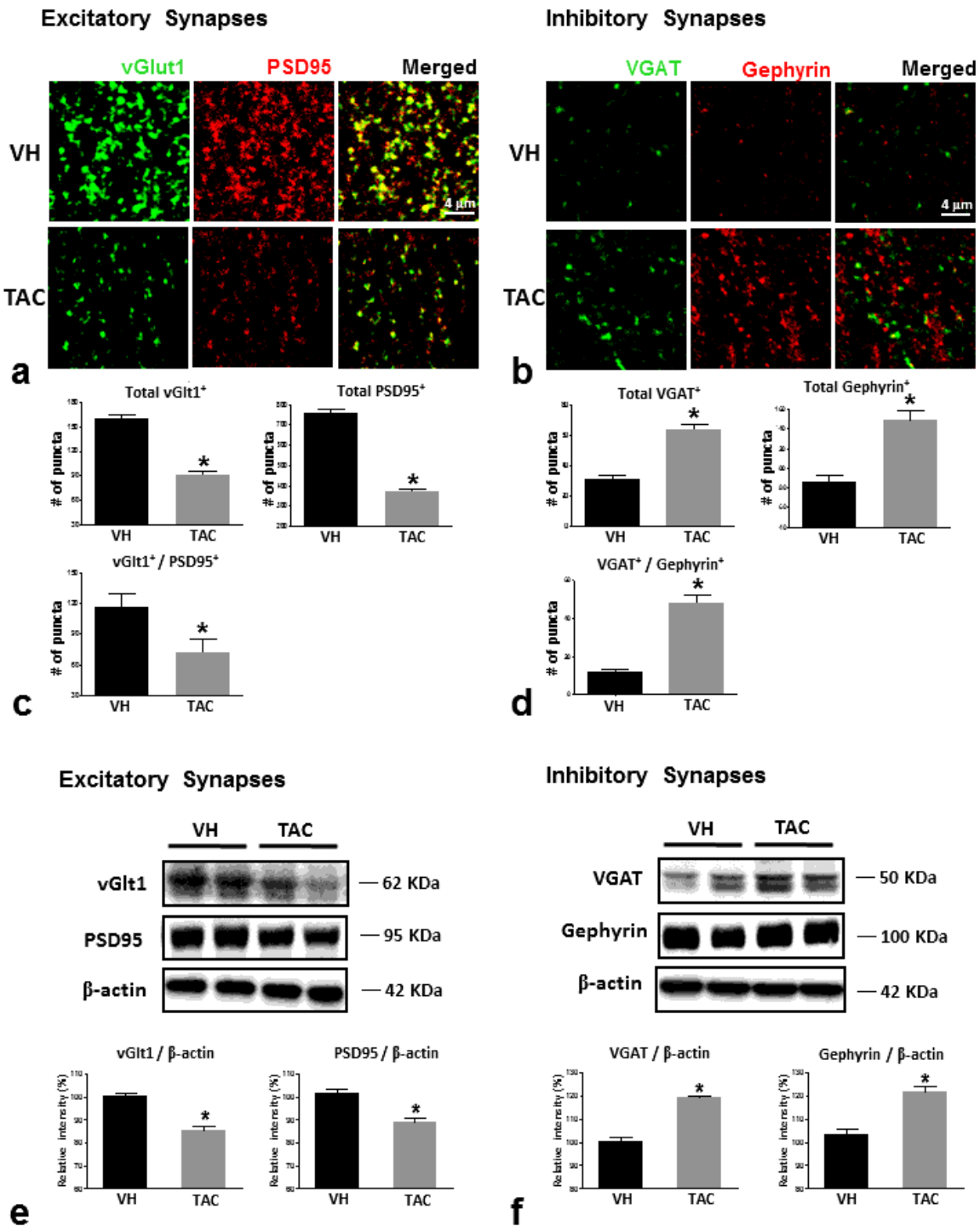

Figure 2

Effects of TAC on the immunoreactive changes in the excitatory and inhibitory synapses of hippocampal neurons. (A–B) Expression of excitatory pre- and postsynaptic markers (vGlut1 and PSD95, respectively) and inhibitory pre- and postsynaptic markers (VGAT and gephyrin, respectively). (C–D) Quantitative analysis of the numbers of the immunoreactive puncta in each markers. vGlut1- and PSD95-expressing excitatory synapses were decreased, whereas VGAT- and gephyrin-expressing inhibitory synapses were increased in the TAC-treated hippocampal neurons, compared with those in the VH group. (E–F) Representative immunoblot and quantification of synaptic markers showed that TAC treatment significantly decreased the excitatory synaptic marker vGlut1 and PSD95 (E), and simultaneously increased the inhibitory synaptic markers VGAT and gephyrin (F). Optical densities of the bands in each lane were normalized with the β-actin optical density from the same gel. The values shown are presented as means ± SE (n = 5). *P < 0.05 vs. VH. Scale bar = 4 μm for A–B.

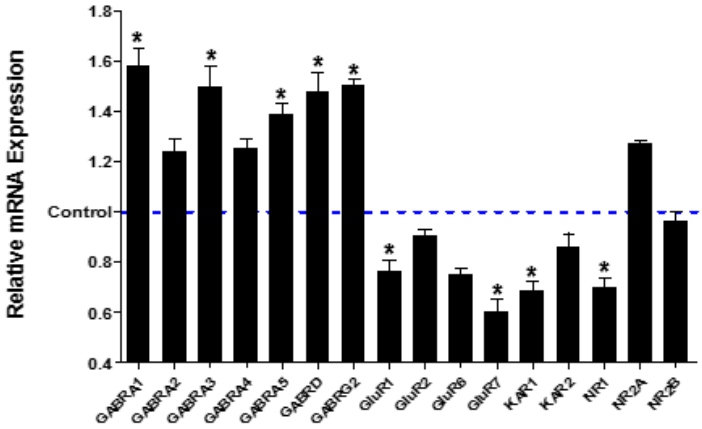

Figure 3

Quantitative analysis for neurotransmitter receptors in the hippocampus of TAC-treated mice. The mRNA expression of neurotransmitter receptors was detected by RT-qPCR in the VH and TAC-treated hippocampus. Relative mRNA expression levels were calculated after normalization to Gapdh expression, and expression levels in VH were considered as the control. The values shown are presented as the mean ± SE (n = 5). *P < 0.05 vs. Control.

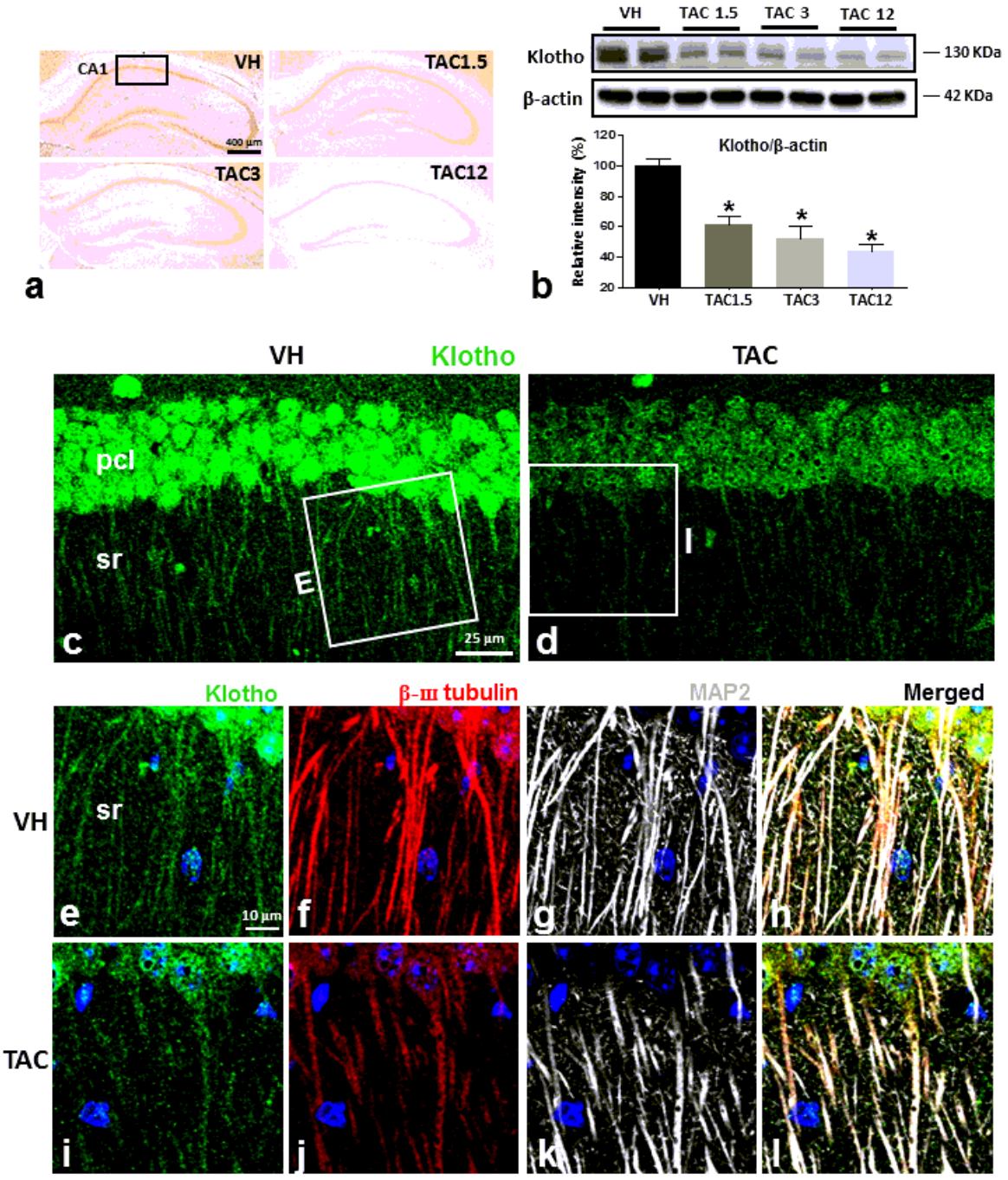

Figure 4

Decreased hippocampal expression of Klotho following chronic TAC treatment. The labeling intensity for Klotho was prominent in the vehicle (VH) groups, compared with the other groups (A). Representative immunoblot and quantification (B) of Klotho shows that TAC treatment significantly decreased the level of Klotho in a dose-dependent manner. Optical densities of the bands in each lane were normalized with the β-actin optical density from the same gel. (C–D) Immunoreactivity for Klotho was detected in the

pyramidal cell layer (pcl) and stratum radiatum (sr) of the CA1 region and the labeling intensity was more prominent in the VH group (C) compared with that in the TAC group (D). (E–L) Triple labeling for Klotho with β-III tubulin, microtubule-associated protein 2 (MAP2), which are both cytoskeleton markers for neurons, indicated that Klotho expression is present in the soma and neurites of hippocampal neurons. (E, I) High-magnification images of the boxed areas in C and D, respectively. The punctate Klotho-labeled profiles were distributed in the stratum radiatum, and are associated with the neurites of hippocampal neurons. pcl, pyramidal cell layer; sr, stratum radiatum. Scale bar = 25 μm for C–D; 10 μm for E–L. The values shown are presented as means ± SE. *P < 0.05 vs. VH. Scale bar = 400 μm for A.

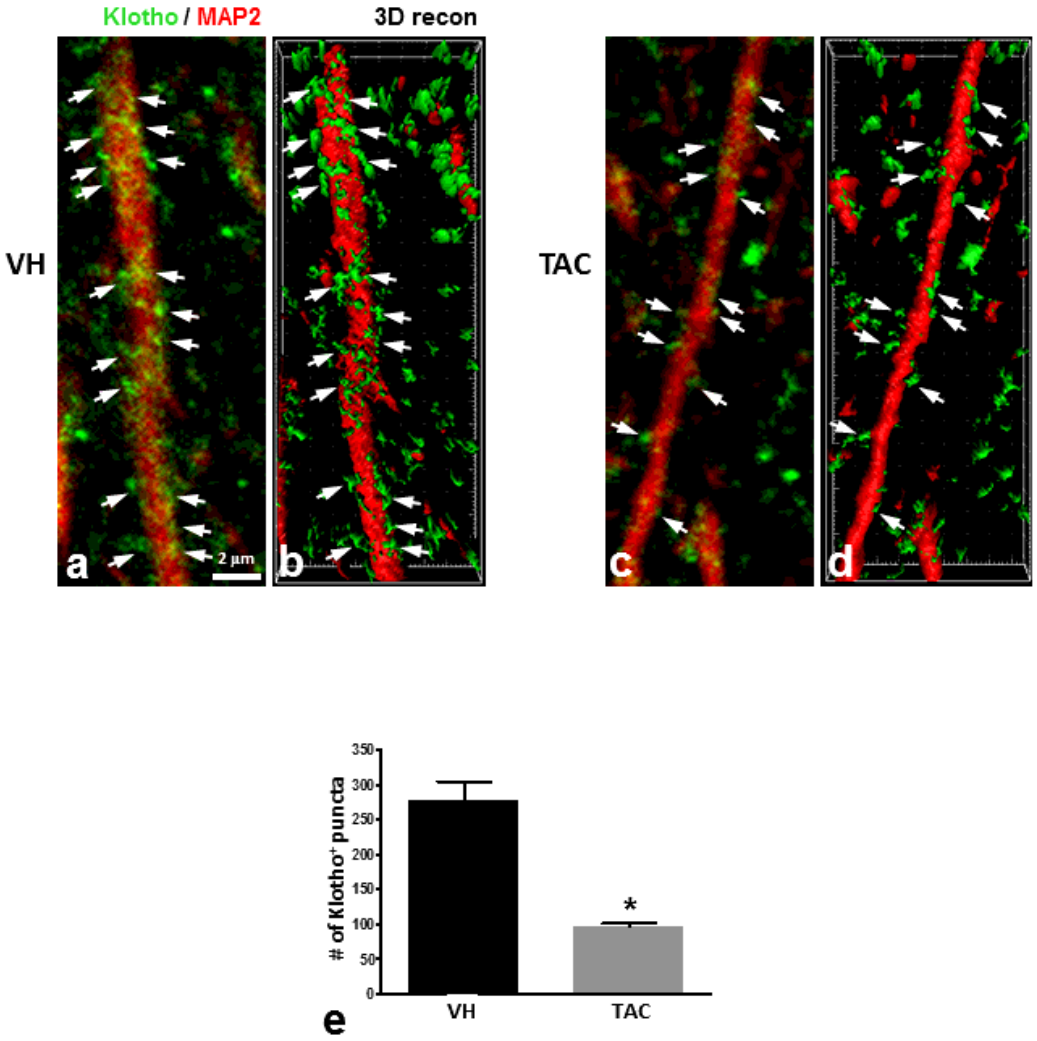

Figure 5

Decreased Klotho expression in the synapse structure of neural dendrites following chronic TAC treatment. (A, C) Double labeling for Klotho and MAP2, a marker of neuronal dendrites, showing that most Klotho-labeled profiles were along the MAP2-positive dendrites. Intense Klotho immunoreactivity was observed in the VH group (A) compared with the TAC group (C). (B, D) Three-dimensional renderings of the images shown in A and C, showing that the punctate structure of Klotho was observed along the

dendrites and that these puncta enclosed the dendrites. Arrows denote the appearance of punctate Klotho immunoreactivity surrounding the dendrite profiles. (E) Quantification of the number of the Klotho-positive puncta in the dendrites. The values shown are presented as means ± SE. *P < 0.05 vs. VH. Scale bar = 2 μm for A–D.

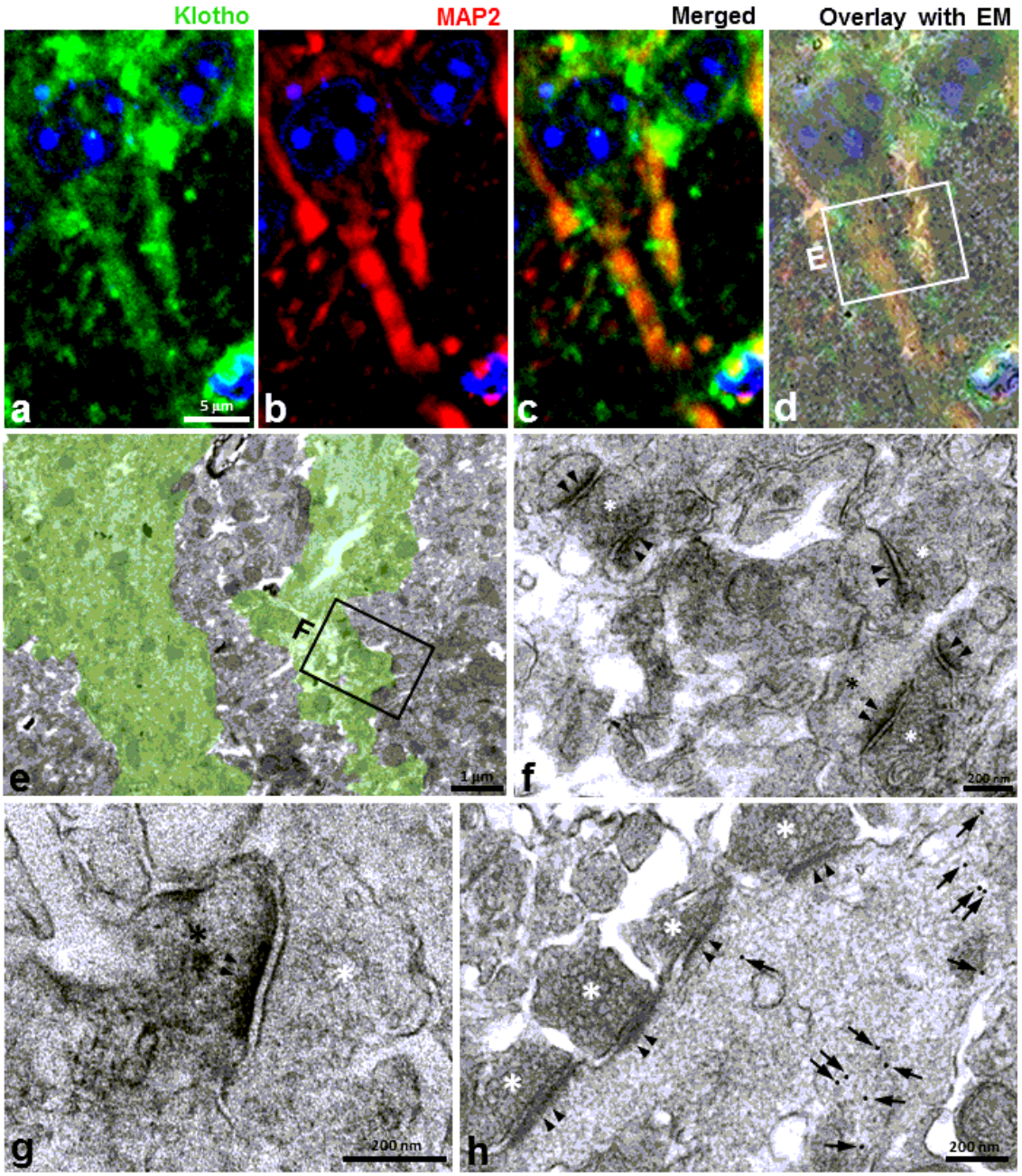

Figure 6

Ultrastructural localization of Klotho in postsynaptic profiles. (A–C) Confocal microscopic image of a semithin section double-labeled with Klotho and MAP2, and overlay image of the confocal microscopic data onto the corresponding electron microscopic image (D). (E) corresponding transmission electron microscopic images obtained from the boxed areas in D. (F) High-magnification views of the boxed areas in E. Klotho was expressed in the MAP2-positive neuronal dendrites; the arrowheads indicate the postsynaptic density (PSD) in the dendrites. (G–H) Pre-embedding immunoelectron microscopic images of Klotho immunostaining obtained using immunoperoxidase (G) and immunogold-silver labeling (H). Klotho-positive electron-dense (black asterisk in G) regions were associated with the postsynaptic profile along with the PSD (arrowheads in G), and were located adjacent to the presynaptic terminals with numerous synaptic vesicles (white asterisk in G). In addition, the silver grains for Klotho (arrows in H) were observed in the dendritic cytoplasm with PSD (arrowheads in H). The white asterisks indicate synaptic vesicles in the presynaptic profiles. Scale bar = 3 μm for A–D; 1 μm for E; 0.5 μm for F; 200 nm for G–H.

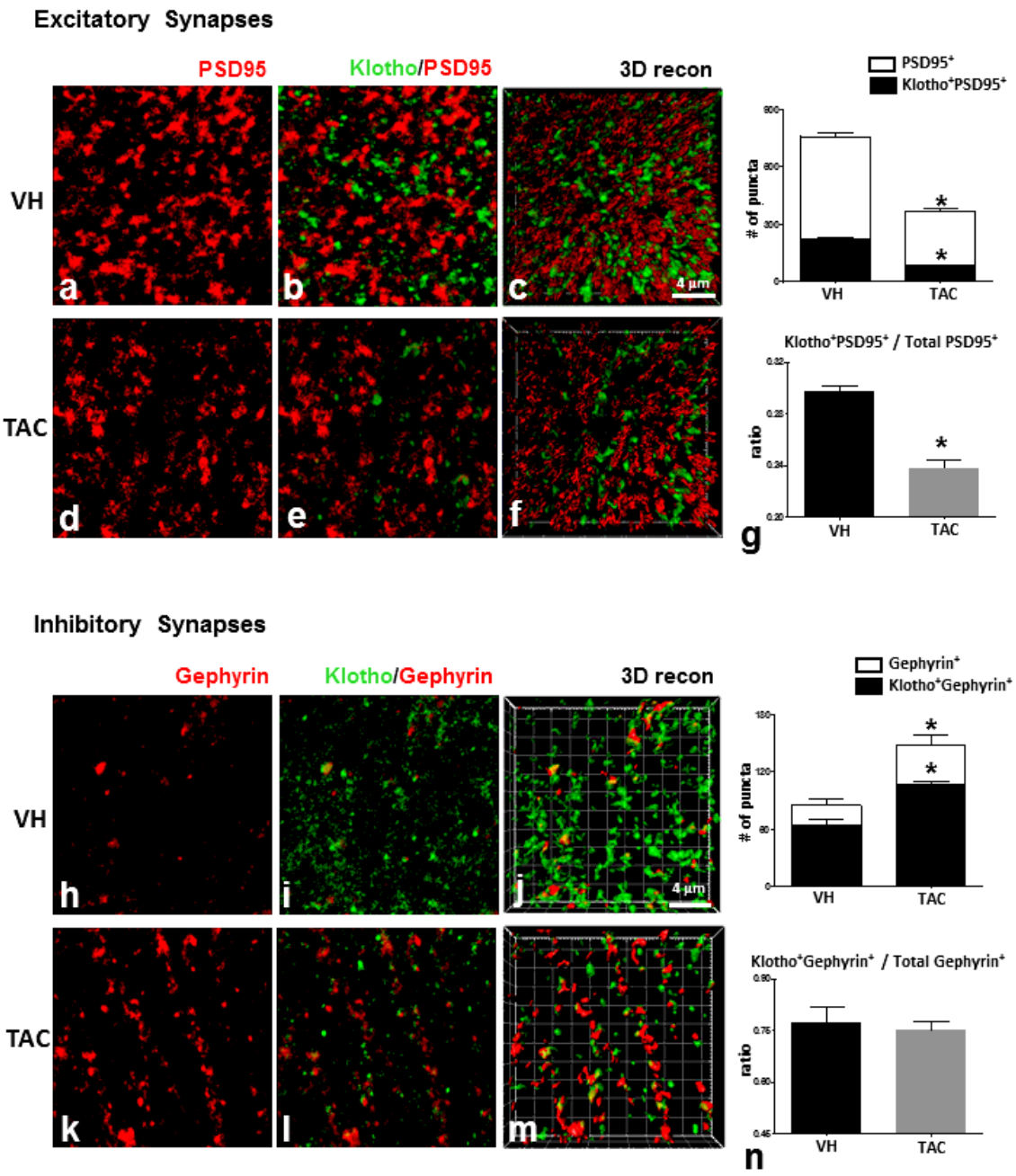

Figure 7

Decreased Klotho expression in the excitatory synapse after TAC treatment. Double labeling for Klotho and PSD95 (A–B, D–E), or Klotho and gephyrin (H–I, K–L), and the respective three-dimensional rendering (C, F, J, M) of the images shown in G-H, and K-L, showing the punctate structure of Klotho in PSD95- or gephyrin-positive synapses, respectively. (G, N) Quantitative analysis of the numbers of the Klotho-positive postsynapses, showing that TAC significantly decreased Klotho expression at the excitatory

synapse, and not at the inhibitory synapse. The values shown are presented as means ± SE. *P < 0.05 vs. VH. Scale bar = 4 μm for A–F, H–M.

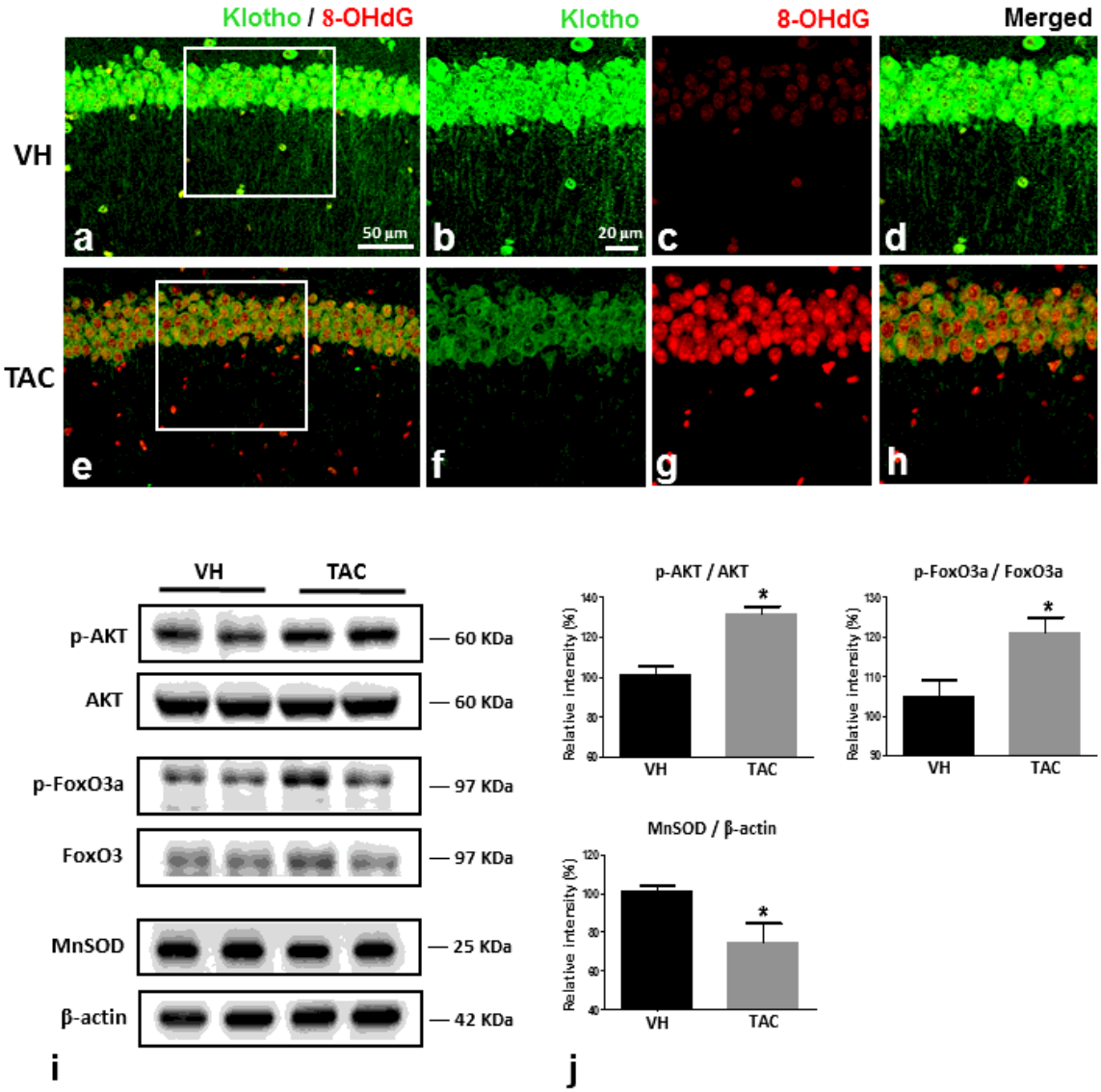

Figure 8

Effect on TAC treatment on oxidative stress in the mouse hippocampus. (A–H) Double labeling for Klotho and 8-OHdG, a marker of oxidative stress, showing that the majority of Klotho-positive neuron profiles was co-expressed with 8-OHdG. Intense 8-OHdG expression was observed in weak Klotho

immunoreactive neurons in the TAC group (A–D) compared with the VH group (E–H). (I–J) Immunoblots for phosphorylated (p)-Akt, p-FoxO3a, and MnSOD, and their quantitative analysis in the experimental groups. Hippocampal p-AKT and p-FoxO3a were increased in TAC-treated mice, whereas MnSOD expression was decreased. The values shown are presented as means ± SE. *P < 0.05 vs. VH. Scale bar = 50 μm for A, E; 20 μm for B–D, F–H.

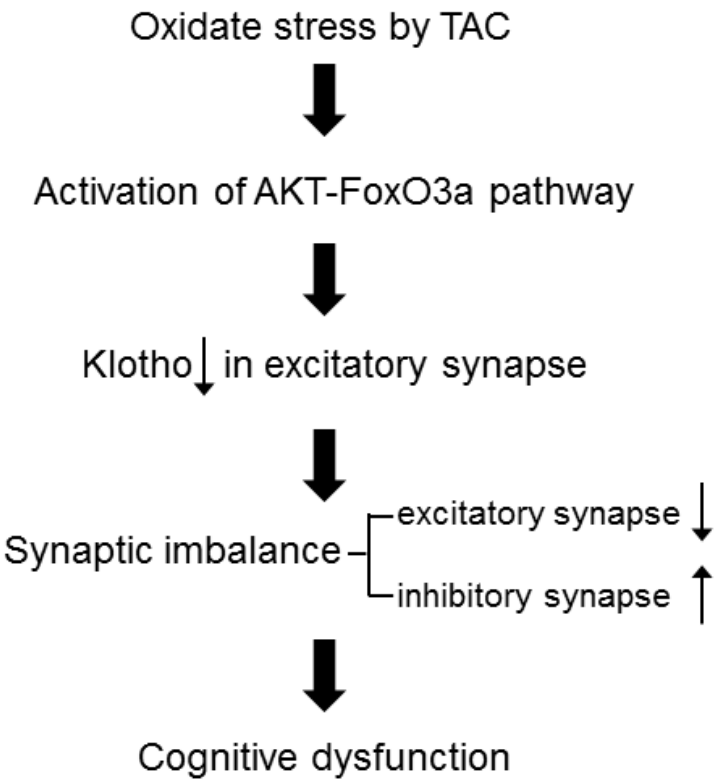

Figure 9

Proposed mechanism of Tac-induced cognitive dysfunction in the hippocampus.